Sphingomyelin biosynthesis is critical in organizing phosphoinositide turnover during phagocytic uptake of *Mycobacterium tuberculosis*

Patrick Niekamp[*1,2], *Gaelen Guzman*[*1], *Hans Leier*[1], *Ali Rashidfarrokhi*[3], *Veronica Richina*[4], *Fabian Pott*[1], *Joost CM Holthuis*[2], *Fikadu G. Tafesse*[1#]

[*]These authors contributed equally.

[1]Department of Molecular Microbiology and Immunology, Oregon Health & Science University, 3181 SW Sam Jackson Park Road, Portland, OR 97239.

[2]Biology & Chemistry Department, University of Osnabrück, Fachbereich Biologie/Chemie, Barbarastrasse 13, 49076 Osnabrück, GERMANY. [3]Department of Pathology and Department of Medicine, New York University Langone, 550 First Avenue, MSB 594, New York, NY 10016.

[4]Department of Biomedicine University Basel Hebelstrasse 20 4031 Basel Switzerland.

[#]Correspondence: tafesse@ohsu.edu

Abstract

Phagocytosis by alveolar macrophages is the obligate first step of infection by *Mycobacterium tuberculosis*, yet the mechanisms of this potential vulnerability in the bacterial life cycle are incompletely understood. Here we show that sphingolipids, a lipid class enriched in the outer leaflet of plasma membranes, are required for *M. tuberculosis* to efficiently enter and infect phagocytes. Genetic knockout or inhibition of serine palmitoyltransferase or ceramide synthases, key enzymes that catalyze the *de novo* sphingolipid biosynthesis, greatly reduces *M. tuberculosis* uptake by diverse phagocytic cell types without affecting other forms of endocytosis. This phenotype is caused by multiple defects in the cellular processes that are critical for the formation of a phagocytic cup. While the clustering of innate immune receptors such as Dectin-1 is normal, the exclusion of the regulatory phosphatase CD45 from the receptor engagement site at the phagocytic synapse is defective in cells deficient in sphingolipid biosynthesis. We also show that the turnover of phosphoinositides and activation of small GTPases at the phagosomal synapse are impaired upon blockade of sphingolipid synthesis. Human monocytes deficient in sphingomyelin biosynthesis show reduced *M. tuberculosis* uptake comparable to that of cells depleted of total sphingolipids, indicating that sphingomyelin is specifically required for phagocytosis. Together, these data identify the sphingomyelin biosynthetic pathway as a critical cellular process mediating the earliest stage of *M. tuberculosis* invasion and establish the significance of this lipid in innate immune responses.

36 **Introduction**

37 The etiologic agent behind an estimated 10 million new cases of tuberculosis and 1.6
38 million deaths in 2017 alone, *Mycobacterium tuberculosis* (Mtb) has established itself as a highly
39 effective and insidious pathogen[1,2]. Mtb invades alveolar immune cells through phagocytosis, and
40 wields an extensive repertoire of effector molecules that operate to dampen the immune response,
41 reprogram the host lipidome, and promote long-term intracellular survival[3,4]. As an intracellular
42 pathogen, Mtb necessarily interacts with its host along numerous lipid interfaces throughout its
43 infectious lifecycle. Understanding the biological roles of host lipids during infection may
44 illuminate novel routes of therapeutic strategies to prevent the onset and spread of tuberculosis[5].

45 In most settings, phagocytosis is critical for clearing dead and effete cells, and serves
46 as a first line of defense against microbial pathogens. This process culminates in the
47 engulfment and internalization of target particles, which are subsequently degraded following
48 convergence of the phagosome with the lysosome[6]. In the context of pathogen clearance, uptake
49 by professional phagocytes (primarily monocytes, macrophages, and dendritic cells) results in a
50 robust inflammatory response and antigen presentation that may contribute to an adaptive immune
51 response[7]. For example, previous work shows that phagocytic uptake of *Candida albicans* is
52 essential for the clearance of infection *in vivo*[8]. In contrast, Mtb is highly adept at subverting its
53 own degradation to survive within phagosome-derived compartments through an array of
54 mechanisms. As one example, this pathogen inhibits the Ca^{2+}-dependent fusion of the phagosome
55 to the lysosome by disrupting the activity of sphingosine kinase[6,9]. Cholesterol is reported to be
56 required for Mtb entry[10]. Despite extensive literature on the host-pathogen interactions of Mtb, the
57 specific functional roles played by host lipid species at the site of initial phagocytic
58 uptake of Mtb have remained relatively unstudied. In particular, structural and signaling functions

59 played by sphingolipids at the cell membrane and within the phagosome during Mtb infection are
60 unknown.

61 Sphingolipids are a complex family of membrane lipids that contain a sphingoid base. A
62 species of particular note, sphingomyelin constitutes a significant fraction of the total lipid
63 composition of the exoplasmic leaflet of the plasma membrane and plays critical roles in the
64 organizing membrane dynamics at the cell surface[11,12]. A growing body of literature shows that
65 sphingolipids mediate functions beyond existing as membrane barrier components: members of
66 this family accumulate in specialized lipid domains and act as secondary messengers within the
67 cell[13–15]. These signaling functions are relevant to many biological processes that span
68 from apoptosis and autophagy to stress response and inflammation in many (if not all) mammalian
69 cell types[16–18]. The cellular proportions of ceramide and spingosine-1-phosphate have been shown
70 to act as a rheostat that determines cell survival under stress[19]. Notably, it has been shown that the
71 biosynthetic flow of sphingolipids through the Golgi creates a regulatory feedback loop that
72 controls the levels of phosphatidylinositol-4-phosphate, although interactions outside of the *trans*-
73 Golgi network are unknown[20].

74 Prior work has investigated the roles played by sphingolipids during the phagocytosis of
75 other particles – contradictory reports describe the effect of sphingolipid depletion during
76 phagocytosis. We have previously reported that cellular sphingolipids are critical for the *in vivo*
77 clearance of *Candida albicans* infection through phagocytosis by macrophages[8]. In contrast,
78 depletion of cellular sphingolipids reportedly enhances phagocytic uptake of opsonized particles[21].
79 Together, these results suggest that the roles played by sphingolipids during phagocytosis may be
80 pathogen or particle specific, based on the specific ligands decorating a particle[22]. However, the
81 role of sphingolipids during entry of Mtb remained poorly understood.

82 Here, we employed chemical and genetic tools to manipulate levels of sphingolipids in
83 mammalian phagocytes, and infected them using an mCherry-expressing reporter strain of H37Rv
84 Mtb. We first show that host sphingolipid depletion reduces the capacity of Mtb to invade host
85 cells through phagocytosis – but that other mechanisms of endocytosis are unaffected. We next
86 show that sphingolipid depletion resulted in the impairment of the regulatory phosphatase CD45
87 displacement by phagocytic receptors at the site of particle engagement. Furthermore, we
88 demonstrate that blockade of sphingolipid biosynthesis results in defects of phagocytic signaling,
89 including an unsuccessful activation and recruitment of the small GTPases Rac1 and CD42 to the
90 phagocytic cup. This in turn resulted in only transient and futile turnover of phosphoinositidyl-4,5-
91 *bis*phosphate, a critical process for actin remodeling during phagosome formation. Finally, we
92 show that specifically inhibiting the *de novo* synthesis of sphingomyelin results in a robust
93 phenocopy of total blockade of sphingolipid biosynthesis. Together, these data demonstrate that
94 intact sphingomyelin biosynthesis is required for the earliest stages of *M. tuberculosis* invasion
95 and highlights the importance of this host lipid in innate immune responses against this pathogen.
96

97 **Results**

98 **Manipulating sphingolipid biosynthesis in mammalian phagocytes using genetic and**
99 **chemical tools**

100 To define the role of the sphingolipid biosynthetic pathway in phagocytic uptake of Mtb,
101 we sought to inhibit sphingolipid biosynthesis in four different phagocytic cell lines: the murine
102 macrophage cell line RAW 246.7, the murine dendritic cell line DC2.4, the human monocyte cell
103 lines THP-1 and U937. We first used a chemical approach to inhibition using the compounds
104 myriocin (Myr) and fumonisin B1 (FB1). As depicted in Figure 1A, the initial and rate limiting
105 step of sphingolipid synthesis is the production of the sphingoid base through the condensation of
106 serine and palmitoyl-CoA, and is performed by the enzymatic complex serine palmitoyltransferase
107 (SPT)[23]. Previously we reported that genetic ablation of Sptlc2 results in blockade of *de novo*
108 synthesis of all sphingolipid, as does treatment with the atypical amino acid Myr[8]. The fungal toxin
109 FB1 acts several steps downstream in the sphingolipid biosynthetic pathway by blocking the
110 activity of ceramide synthase[8]. As the central nexus of sphingolipid synthesis, ceramide is
111 converted into many classes of higher sphingolipids - including sphingomyelin,
112 glycosphingolipids, and galactosylceramides[19,24].

113 To verify the reported effects of myriocin and fumonisin B1 and Sptlc2 knockout, we used
114 thin layer chromatography to visualize the incorporation of 3-L-[^{14}C]-serine into sphingolipid
115 species in RAW 246.7, THP-1, DC2.4, and U937 cells following 3-day treatment with Myr and
116 FB1 (Figure 1B and D and Supplementary Figure 1). Across all cell lines, treatment with these
117 compounds resulted in significant reduction of sphingolipid content, without disrupting
118 phosphatidylserine content – demonstrating the specificity and potency of these compounds
119 (Figure 1E and F).

120 To further examine the lipid composition of cells deficient in sphingolipid biosynthesis,
121 we performed mass spectrometry-based lipidomic analysis of RAW 264.7 macrophages following
122 treatment with chemical inhibitors and Sptlc2 knockout. We examined cellular levels of
123 sphingosine, ceramide, sphingomyelin, and glucosylceramide. As expected, both myriocin and
124 Sptlc2 knockout result in significant reduction of all sphingolipid species (Figure 1 G-J). In FB1
125 treated cells, we observe reduction of all sphingolipid species downstream of ceramide synthesis
126 (the point of inhibition along the biosynthetic pathway), but we observe a concordant increase in
127 sphingosine (synthesized upstream of ceramide), as previously reported (Figure 1G-J)[25].
128 We then sought to verify the mutation in Sptllc2 gene or inhibitor treatments do not have a
129 pleiotropic effect. To this end, we carefully examined for any defect in the overall viability and
130 morphology of the cell. Despite a reduced level of sphingolipids, these cells grow normally with
131 no apparent defect in morphology or viability (Supplementary Figure 2). Notably, we observe
132 that myriocin and FB1 treatment, as well as Sptlc2 knockout, do not result in the total ablation of
133 cellular sphingolipid content. This is at least partially attributable to the activity of the
134 sphingolipid salvage pathways, through which cells may acquire sphingolipids from additives in
135 media – primarily serum. It is likely that cells deficient in sphingolipid biosynthesis acquire
136 sphingolipids from media at only the minimal level to allow cell growth, as their overall
137 sphingolipid content is significantly lower than in wildtype cells (Figure 1D-J). This is consistent
138 with our previous report that shows the Sptlc2$^{-/-}$ DC2.4 cells do not harbor any significant defect
139 with regards to cell survival, morphology, and membrane trafficking [8]. As described below, the when
140 grown in the presence of serum, the primary phenotype following blockade of sphingolipid
141 biosynthesis is a reduced rate of phagocytic uptake of pathogens such as Mtb.
142

143 **Cells deficient in sphingolipid biosynthesis display reduced capacity to phagocytose Mtb.**

144 To investigate the role of sphingolipids during phagocytic uptake of Mtb, we used Myr and
145 FB1 to block sphingolipid synthesis in RAW 264.7, THP-1, DC2.4, and U937 cells. We then
146 infected cells with an mCherry-expressing strain of Mtb to quantify rates of phagocytosis. Figure
147 2A depicts the experimental and analysis workflow. Briefly, cells were infected at a multiplicity
148 of infection (MOI) of 10 for two hours, after which cells were fixed and stained with DyLight 488-
149 conjugated phalloidin and with DAPI (to visualize F-actin at cell boundary and nuclei,
150 respectively). Fluorescence microscopy was used to quantify uptake efficiency through automated
151 counting of cell number (by nuclei) and internalized bacteria (red fluorescent particles within green
152 cell boundary). We report uptake efficiency as the ratio of the total number of internalized Mtb
153 particles against the number of identified nuclei, and normalized the uptake rate of treated cells to
154 that of untreated cells to address variability between biological replicates. In all cell models
155 analyzed, we observed a statistically significant reduction in Mtb uptake of approximately 50%
156 following treatment with myriocin, and approximately 40% for FB1 (Figure 2B-I). Similarly, the
157 knockout of Sptlc2 resulted in approximately 50% of wildtype uptake in both RAW 264.7 and
158 DC2.4 cells (Figure 3A-D). These results suggest that the maintenance of total cellular
159 sphingolipid levels through active sphingolipid biosynthesis is required for efficient phagocytic
160 uptake of Mtb across four model cell lines and irrespective of the mechanism of inhibition.

161 We next sought to assess whether blocking sphingolipid biosynthesis affects the
162 phagocytosis of Zymosan A, a model particle composed of β-glucan chains derived from
163 Saccharomyces cerevisiae. Zymosan A particles engage the C-type Lectin receptor Dectin-1,
164 expressed on professional phagocytes[8,26,27]. Dectin-1 is one of several pathogen recognition
165 receptors that engage Mtb and initiate phagocytic signaling to facilitate host cell entry[28,29]. We

166 thus hypothesized that inhibiting sphingolipid biosynthesis in host cells would result in a reduced
167 uptake rate for this Zymosan A, reflecting that of Mtb. We found that Sptlc2-deficient RAW 264.7
168 cells are reduced in their capacity to uptake Zymosan A to a similar degree as to that of Mtb uptake
169 (Figure 3E and F). We thus used Zymosan A as a model particulate to gain further insight regarding
170 the mechanism in which sphingolipids are involved in phagocytosis.

171 **Sphingolipid-depleted cells are permissive to virus that utilizes phagocytosis-like cellular**
172 **processes.**

173 Are the effects of sphingolipid depletion restricted to phagocytic uptake? To answer this
174 question, we performed parallel infections of RAW 264.7 wildtype and Sptlc2 knockout cells using
175 a fluorescent reporter strain of Herpes Simplex Virus-1 (HSV) encoding a fusion of viral protein
176 VP26 and mCherry[30]. HSV is an enveloped virus that gains entry to host cells through the
177 phagocytosis-like process of macropinocytosis, and the viral receptors have been shown to be
178 nectin-1 (also known as herpesviruses entry mediator)[31,32]. It has been shown that HSV entry is
179 dependent on cholesterol and dynamin2[33]. At 12-hours post-infection, we visualized and quantified
180 rates of infection using high-content imaging as described above. Because the VP26-mCherry
181 reporter construct localizes to the nucleus, we did not stain cells using phalloidin and instead used
182 the co-localization of DAPI with mCherry as a measure of infection. We observe that there is no
183 significant difference in the infection rates of wildtype and Sptlc2$^{-/-}$ cells, suggesting that
184 sphingolipids play no significant role in the entry of HSV-1 (Figure 3G and H). These data
185 demonstrate that endocytic pathways are functional in sphingolipid-deficient cells, suggesting a
186 specific role for sphingolipids in phagocytosis of bacterial pathogens such as Mtb by immune
187 cells.

188

189 **The exclusion of the regulatory phosphatase CD45 from the site of particle engagement is**
190 **impaired in Sptlc2$^{-/-}$ cells**

191 It has been shown that the engagement of phagocytic receptor to ligand initiates the
192 accumulation of pathogen recognition receptors to the phagocytic synapse, which results in the
193 physical expulsion of inhibitory phosphatases such as CD45 from the phagocytic synapse and the
194 formation of a lipid raft-like domain[34]. Prior work has shown that the several intracellular
195 pathogens, including Mtb, induce their uptake in a cholesterol-dependent manner[5,35]. Because
196 sphingolipids such as sphingomyelin have been shown to play a role in the formation of both lipid
197 raft and cholesterol-rich domains, we hypothesized that cellular sphingolipid content is required
198 for the aggregation of the pathogen recognition receptor Dectin-1 to the site of particle
199 engagement, and the concomitant exclusion of CD45 from the contact site.

200 To address this hypothesis, we transiently transfected wildtype and Sptlc2$^{-/-}$ RAW 264.7
201 macrophages with a GFP-tagged Dectin-1 construct, and assessed the co-localization of this
202 fluorescent protein with the inhibitory phosphatase CD45 upon treatment with non-fluorescent
203 Zymosan A particles two minutes post-incubation. In both wildtype and Sptlc2 knockouts, we find
204 that Dectin-1 aggregates at the site of contact with Zymosan A within the first two minutes. As
205 expected, in wildtype cells the inhibitory phosphatase CD45 is efficiently displaced by Dectin-1.
206 To this end, the co-localization of CD45 with Dectin-1 in wildtype cells is significantly reduced at
207 the site of particle engagement (Figure 4A and B). In contrast, the co-localization of Dectin-1-GFP
208 and CD45 in Sptlc2 knockout cells is only minimally reduced (Figure 4A and B). These data
209 suggest that sphingolipid biosynthesis is required to mediate the proper displacement of CD45, a
210 step that is critical for the initiation of phagocytic synapse formation.

211 To control against the possibility that deficient sphingolipid biosynthesis results in altered
212 surface expression of CD45 and Dectin-1, we used flow cytometry to compare surface expression
213 of these proteins between wildtype and Sptlc2$^{-/-}$ RAW 264.7 cells. We probed cells for endogenous
214 surface protein using APC-conjugated anti-CD45 antibody and FITC-conjugated anti-Dectin-1
215 antibody. We found agreement in overall fluorescent signal for both wildtype and Sptlc2 knockout
216 cells for both surface markers (Figure 4C-F). These results suggest that the levels of both CD45
217 and Dectin-1 at the cell surface are unaffected by blocking the biosynthesis of sphingolipids.
218
219 **Activation of Rho GTPases Rac1 and Cdc42 are defective in Sptlc2$^{-/-}$ cells.**
220 As we describe above, the initial stages of phagosomal synapse formation are impaired in
221 Sptlc2$^{-/-}$ cells. Downstream of receptor activation, phagocytosis is strictly regulated through a
222 signaling network that involves the dynamic activation and recruitment of both enzymes (such as
223 GTPases, kinases, and phosphatases) and lipids – particularly several phosphatidylinositol species.
224 To determine whether blocking sphingolipid biosynthesis perturbs downstream phagocytic
225 signaling events following particle engagement, we transfected wildtype and Sptlc2$^{-/-}$ cells with
226 Rac1/Cdc42 fluorescent biosensors to examine the activation and localization of these proteins
227 during phagocytosis.
228 As depicted in Figure 5A, the Rho GTPases Rac1 and Cdc42 are activated via
229 phosphorylation following engagement of phagocytic receptors to pathogenic particles such as
230 Mtb[36]. To visualize the activation of these GTPases, we transfected wildtype and Sptlc2$^{-/-}$ RAW
231 264.7 macrophages with a fluorescent biosensor consisting of the fusion of YFP to the p21-binding
232 domain of the p21-activated kinase (PBD(PAK)-YFP) – this biosensor enables the visualization
233 of localized GTPase activation[37,38]. Twenty-four hours after transfection, we infected cells using

234 Zymosan A particles at an MOI of 10 and performed live imaging to visualize the distribution of
235 PBD(PAK)-YFP in these cells. In wildtype cells, we observe increased localization of fluorescent
236 signal to the site of particle contact – corresponding to the expected pattern of Rac1/Cdc42
237 activation (Figure 5B and C, and Supplementary Movie1). In Sptlc2$^{-/-}$ cells on the other hand, we
238 observed only a transient (and futile) activation which resulted in significantly reduced
239 accumulation of a sustained fluorescent signal in Sptlc2$^{-/-}$ cells, suggesting that these cells are
240 defective in the activation of Rho GTPases following particle binding (Figure 5B and C, and
241 Supplementary Movie2).
242
243 **Phosphatidylinositol turnover is impaired in Sptlc2 knockout cells.**
244 Next, we visualized the turnover of phosphatidylinositols at the phagocytic synapse. Rho
245 GTPase activation initiates the conversion of phosphatidylinositol-4-phosphate (PIP) to
246 phosphatidylinositol-4,5-*bis*phosphate (PIP2) at the base of the phagocytic synapse. The
247 accumulation of PIP2 is essential to initiate the polymerization of actin filaments that drive the
248 leading edges of the growing phagosome around the particle[38]. Following the leading edge of PIP2
249 production, the enzyme phosphatidylinositol 3-kinase (PI3K) converts PIP2 into
250 phosphatidylinositol-3,4,5-*tris*phosphate (PIP3), which initiates a trailing edge of actin
251 disassembly at the base of the phagosomal cup (Figure 5A)[7]. To date, there have been no reports
252 connecting phosphoinositide signaling to cellular sphingolipid biosynthesis during phagocytosis.
253 However, sphingolipid and phosphoinositide levels within the Golgi regulate each other in a
254 homeostatic feedback circuit: buildup of sphingomyelin in the Golgi initiates dephosphorylation
255 of PI4P, which subsequently reduces the import of cholesterol sphingolipid into the Golgi[20,39].

256 To visualize turnover of these signaling molecules, we transfected RAW 264.7 wildtype
257 and Sptlc2 knockout cells with biosensors that specifically bind PIP2 and PIP3, and used live
258 imaging to examine their dynamics during phagocytois of Alexa55 labeled Zymosan A particles.
259 The first such biosensor we used consisted of the fusion of GFP to the plekstrin homology (PH)
260 domain of phospholipase C-delta (PLCδ), which selectively binds to PIP2 (PH(PLCδ)-GFP)[7]. We
261 show an enrichment of GFP signal to the site of particle engagement as wildtype cells synthesize
262 PIP2 following particle recognition, and that this synthesis peaks with the engulfment of the
263 particle (Figure 5D and E and Supplemental Movie 3). In Sptlc2$^{-/-}$ cells, however, we observe only
264 a transient (and futile) accumulation of GFP signal and fails to accumulate to the same degree as
265 in wildtype cells – and thus appear fail to synthesize PIP2 (Figure 5D and E and Supplemental
266 Movie 4).

267 We then transfected RAW 264.7 cells with a PIP3 biosensor consisting of the PH domain
268 of Akt fused to GFP (PH(AKT)-GFP)[40]. We visualized the localization of biosensor signal to show
269 that wildtype cells begin synthesizing PIP3 early in phagocytosis, and that this synthesis strongly
270 peaks as a particle is fully engulfed (Figure 5F and G and Supplementary Movie 5). However,
271 Sptlc2 knockout cells fail to produce a trailing wave of PIP3, and thus never reach the levels of
272 synthesis observed in wildtype cells (Figure 5F and G and Supplementary Movie 6).

273 Together, these results support the hypothesis that active sphingolipid biosynthesis is
274 required for the initiation of the phagocytic signaling cascade, as well as for the transduction of
275 pro-phagocytic signaling.

276

277 **Sphingomyelin biosynthesis is required for efficient Mtb uptake**

278 Which sphingolipid is most essential for enabling phagocytic signaling? Because
279 sphingomyelin is highly enriched to the exoplasmic leaflet of the plasma membranes, we
280 hypothesized that this lipid species is responsible for reduced Mtb uptake in cells depleted of total
281 sphingolipids[11,24,41]. Sphingomyelin constitutes a major branch of the sphingolipid biosynthetic
282 pathway, and the majority of its synthesis is catalyzed by the enzyme sphingomyelin synthase 1
283 (SGMS1) in the Golgi – as such, cells may be depleted of this specific lipid species through
284 CRISPR/Cas9-mediated knockout of this gene. Two SGMS1 CRISPR/Cas9 knockout clones of
285 U937 cells that were isolated as previously described[42]. Using these SGMS1 knockouts, we
286 performed Mtb uptake assays as described above. We found that SGMS1$^{-/-}$ cells are reduced in
287 their capacity to uptake Mtb to a similar degree as to that of cells deficient in the biosynthesis of
288 all sphingolipids (Figure 6A and B, and Figure 2A and B).

289 To address the possibility that other sphingolipids beyond sphingomyelin play roles in the
290 phagocytosis of Mtb, we used CRISPR-Cas9 to knock out UDP-glucose ceramide
291 glycosyltransferase (UGCG) in THP-1 cells (Figure 6C and D). UGCG is singularly responsible
292 for catalyzing the synthesis of glucosylceramide – which is in turn the precursor of complex
293 glycosphingolipids, a branch of sphingolipid biosynthesis comprising over 400 known lipid
294 species[43]. If any of these species play a significant role in the phagocytic uptake of Mtb, we
295 hypothesized that the inhibition of glycosphingolipid synthesis would result in a decrease in Mtb
296 internalization. We found that two UGCG$^{-/-}$ clones displayed no change in the rate of Mtb
297 phagocytosis, as compared to wildtype THP-1 cells (Figure 6C and D). Together, these data
298 suggest that sphingomyelin is particularly essential for the phagocytic uptake of Mtb.

299

300 **Discussion**

301 In this study, we report that the capacity of Mtb to invade host cells by engagement of
302 phagocytic receptors is significantly dependent on active sphingolipid biosynthesis pathway. Our
303 central findings are thus: First, the blockade of total sphingolipid synthesis reduces Mtb uptake by
304 approximately 50%. Critically, we show that blocking sphingolipid biosynthesis has no effect on
305 the macropinocytosis of Herpes Simplex Virus – suggesting that these cells remain otherwise
306 susceptible to infection via other routes of cellular uptake. We next show that blocking
307 sphingolipid synthesis results in defects in the exclusion of the regulatory phosphatase CD45 at
308 the phagocytic synapse. Furthermore, we show that several critical stages of phagocytic signaling
309 involving GTPase activation and phosphoinositide turnover are perturbed upon depletion of
310 sphingolipid synthesis, resulting in defective phagosome formation. And finally, we show that the
311 blockade of sphingomyelin synthesis produces a phenocopy of total sphingolipid depletion –
312 suggesting that sphingomyelin specifically is an essential lipid factor during Mtb uptake.

313 These data support a model in which sphingolipids are essential for successful activation
314 of signaling events upon binding of pathogen-particles such as Mtb – and are thereby critical in
315 initiating phagocytic synapse. Sphingolipids are instrumental in the accumulation of activated
316 pathogen recognition receptor at the site of particle binding. This receptor accumulation is in turn
317 essential for activating the phagocytic signaling cascade – including the activation of Rho GTPases
318 and the turnover of phosphoinositides. Without active sphingolipid biosynthesis, there is an overall
319 defect in phagosome formation and a reduction in phagocytic uptake of Mtb – though we find it
320 notable that the lack of sphingolipid biosynthesis does not completely ablate the invasive
321 phagocytosis of Mtb. We postulate that this may be partially due to the activity of the sphingolipid
322 salvage pathways, which allow cells to acquire high-order sphingolipids from the surrounding

323 environment (e.g. fetal calf serum in growth media) and incorporate these species into the cellular
324 lipid pool. Ongoing work seeks to address this hypothesis.

325 This study represents the first evidence for sphingolipids as regulators of signaling during
326 phagocytosis of particles such as Zymosan and Mtb. We have previously reported that active
327 sphingolipid biosynthesis is critical for the phagocytic clearance of *Candida albicans* both *in vitro*
328 and *in vivo* – though we found no insight into the mechanism behind this defect in uptake. Further,
329 a recent report suggests that treatment with FB1 results in reduced entry of *M. smegmatis* by
330 J774A.1 cells (whereas there was no effect on the entry of *E. coli*)[44]. Adding an additional layer of
331 complexity, another study suggests that blocking sphingolipid synthesis via treatment with FB1
332 results in enhanced phagocytosis of opsonized particles[22]. We postulate that these data suggest a
333 paradigm in which sphingolipids serve differing roles during the phagocytic uptake of different
334 particles: enhancing the internalization of some, and limiting that of others.

335 Together, we show the dependency of Mtb on the sphingolipid biosynthetic pathway to
336 efficiently enter and invade the host cells. In this context, phagocytosis represents a double-edged
337 sword: while this immune process is critical for the clearance of many pathogenic particles, Mtb
338 harnesses phagocytosis to gain entry to host cells and establish long-term survival. This study
339 represents an important step towards understanding the underlying mechanisms of cellular
340 processes mediating the earliest stage of Mtb invasion and contributes to the development of new
341 strategies to fight this ancient pathogen.

342

Acknowledgements

This work is supported through the National Institutes of Health (3R21AI124225-01A1) and the Medical Research Foundation. We would like to thank the labs of Dr. David Underhill (Cedars-Sinai Medical Center, Los Angeles, CA), Dr. Sergio Grinstein (The Hospital for Sick Children Research Institute, Toronto, ON), Dr. Sebastian Winter (Max Planck Institute of Biochemistry, Munich, Germany), Dr. Tim Nice (Oregon Health and Science University, Portland, OR), and Dr. David Johnson (Oregon Health and Science University, Portland, OR) for kindly providing reagents, cell lines, viruses, and plasmid constructs essential to the completion of this study. We would also like to thank the members of the OHSU Cores for Advanced Light Microscopy and Flow Cytometry for assistance and training in data collection and analysis – in particular, we would like to thank Dr. Stefanie Kaech Petrie, Matthew Lewis, and Sara Christensen. We would finally like to thank Madeleine Faucher, Marie Foss, and Jossef Osborn who kindly and patiently assisted in the editing and preparation of this work.

Conflicts of interest

The authors have no conflicts of interest to declare.

364 **Materials and Methods**

365 **Reagents.**

366 Myriocin and FB1 were purchased from Cayman Chemical Company. 3-L-[^{14}C]-serine
367 was purchased from American Radioactivity. Phorbol 12-myristate 13-acetate (PMA) was
368 purchased from BioLegend. 4% paraformaldehyde was from Fisher Scientific. DyLight® 488
369 Phalloidin was purchased from Cell Signaling Technology, and Alexa Fluor 647-conjugated
370 Zymosan A (*S. cerevisiae*) BioParticles were purchased from Thermo Fisher. Mouse Monoclonal
371 antibody against GAPDH (ab8245) was purchased from Abcam. Anti-rabbit IgG HRP-linked
372 antibody and anti-mouse IgG HRP-linked antibody were purchased from Cell Signaling. APC-
373 conjugated, rat monoclonal antibody against CD45 antibody (Clone 30-F11) was purchased from
374 Biolegend. FITC-conjugated, rat monoclonal antibody against Dectin-1 (Clone 2A11) was
375 purchased from AbD Serotec. Zombie Aqua™ Fixable Viability Kit (part #77143) was purchased
376 from BioLegend.

377

378 **Plasmids**

379 The plasmids used for generation of lentivirus consists of the pCDH-CMV(-)-sgRNA plasmid, the
380 psPAX2 (packaging) and pMD2.G (envelope) plasmids. pCW-Cas9 lentivirus was purchased from
381 Addgene. The pMXsIP-Dectin-1-GFP was kindly provided by the lab of Dr. David Underhill
382 (Cedars-Sinai Medical Center, Los Angeles, CA)[45]. Active (GTP-bound) Rac1/Cdc42 was
383 detected with PAK(PBD)-YFP, a plasmid encoding the PBD of PAK fused to YFP[37] was obtained
384 from Addgene. PI(4,5)P2 was detected with PH(PLCδ)-GFP, a plasmid encoding the PH domain
385 of PLCδ fused to GFP. PI(3,4,5)P3 levels were monitored by PH(AKT)-GFP, a plasmid encoding

386 the PH domain of AKT fused to GFP[46]. These two fusion constructs were kindly provided by the
387 lab of Dr. Sergio Grinstein (The Hospital for Sick Children Research Institute, Toronto, ON).
388
389 **Cell culture and small molecule inhibitor treatment**
390 THP-1, U937, and DC2.4 cells were routinely cultured in RPMI medium supplemented
391 with 10% FBS (Seradigm) and 1% Pen Strep (Gibco). RAW 264.7 cells were cultured in DMEM
392 supplemented with 10% FBS and 1% PenStrep. All cell lines were cultured at 37 °C and 5% CO_2.
393 In plating adherent cells (RAW 264.7 and DC2.4), cells were lifted using 0.25% trypsin solution
394 (Gibco) and counted using hemocytometer, with Trypan Blue solution (Gibco) for counterstain.
395 THP-1 and U937 cells were differentiated to macrophages by 50ng/ml PMA for 1 day in
396 RPMI medium supplemented with 10% FBS, after which the cells were treated with 5μM myriocin
397 or FB1 for 3 days in RPMI supplemented with 10% FBS and 1%Pen Strep. RAW 264.7 and DC2.4
398 cells were treated similarly with myriocin and FB1 – however, 24-hours before infection, cells
399 were lifted and counted, and seeded at appropriate density in 96-well plates or on coverslips.
400 Biological replicates represent independent treatments with chemical inhibitors and infections on
401 separate days.
402
403 **Metabolic labeling and thin layer chromatography**
404 $5x10^5$ cells (wildtype, knockout, or inhibitor-treated) were seeded into a 6-well plate. Cells
405 were labeled with 1μCi/ml of 3-L-[^{14}C]-serine for 4 hours in Opti-MEM supplemented with the
406 appropriate inhibitors. Cells were then washed two times with PBS and lipid extraction was done
407 following the Bligh and Dyer method[47]. The methanol/chloroform-lipid extracts were dried by
408 nitrogen gas. Dried lipids were re-dissolved in several drops of chloroform/methanol (1:2, vol/vol)

409 and loaded on a TLC plate. Lipids were separated by developing the TLC plate first in acetone and
410 then in a mixture of chloroform, methanol and 25% ammonia solution (50:25:6, vol/vol/vol).
411 Radiolabeled lipids were detected on a Storm 825 Phosphor-Imager (GE Healthcare).
412

413 **Generation of lentiviruses**

414 Lentivirus production was performed as described previously[48]. Briefly, lentiviruses were
415 produced by co-transfection of HEK 293T cells with the lentiviral vectors that contain our gene of
416 interest (pCDH-sgRNA or pCW-Cas9) and the packaging plasmids (psPAX2 and pMD2.G).
417 Transfection was performed with Lipofectamine 3000 (Thermo Fisher) according to
418 manufacturer's instructions. Cells were cultured in DMEM supplemented with 10%FBS and the
419 growth medium was replaced after 6 hours. 48 hours after transfection, lentivirus-containing
420 supernatants were harvested, centrifuge for 5min at 1250 rpm and filtered through a 0.45µm filter.
421

422 **Generation of CRISPR/Cas9-mediated knockout cell lines**

423 CRISPR/Cas9-mediated genome-editing for genes involved in the sphingolipid pathway
424 were performed as described previously[8]. Briefly, to generate Sptlc2$^{-/-}$ knockout RAW 264.7 cells
425 were infected with lentivirus (pCW-Cas9) encoding Cas9 cDNA, and were cultured in media
426 containing 2 µg/mL of puromycin (Sigma Aldrich). Potential target sequences for CRISPR
427 interference were found with the rules outlined in Mali et al. 2013[49]. The following seed sequences
428 (CRISPR target sequences) preceding the PAM motif that were found in the exon of Sptlc2 gene
429 were used: Sptlc2 #1 GAACGGCTGCGTCAAGAAC; Sptlc2 #2:
430 AGCAGCACCGCCACCGTCG; UGCG GCTGTGGCTGATGCATTTCA. Potential off-target
431 effects of the seed sequence were evaluated using the NCBI Mus musculus Nucleotide BLAST.

432 Generation of CRISPR/Cas9-mediated Sptlc2-knockout RAW 264.7 cell line and UGCG-
433 knockout THP-1 cell line were performed as previously described[48]. Briefly, CRISPR gBlock was
434 designed to clone into the restriction enzymatic site NheI/BamHI of pCDH-CMV(-) (SBI;
435 CD515B-1) as follows:

436 cacagtcagacagtgactcaGTGTCACAgctagcTTTCCCATGATTCCTTCATATTTGCATAT
437 ACGATACAAGGCTGTTAGAGAGATAATTAGAATTAATTTGACTGTAAACACAAAGA
438 TATTAGTACAAAATACGTGACGTAGAAAGTAATAATTTCTTGGGTAGTTTGCAGTTT
439 TAAAATTATGTTTTAAAATGGACTATCATATGCTTACCGTAACTTGAAAGTATTTCG
440 ATTTCTTGGCTTTATATATCTTGTGGAAAGGACGAAACACCGnnnnnnnnnnnnnnnnnnnG
441 TTTTAGAGCTAGAAATAGCAAGTTAAAATAAGGCTAGTCCGTTATCAACTTGAAAAA
442 GTGGCACCGAGTCGGTGCTTTTTTTggatccTGTGCACAgtcagtcacagtcagtctac (n: CRISPR
443 target sequences).

444 The gBlock was then digested using the restriction enzymes NheI and BamHI and ligated
445 into pCDH-CMV(-) vector that was linearized by digesting with the same restriction enzyme.

446 The Cas9-inducible cells were infected with lentivirus carrying pCDH-CMV(-)-sgRNA,
447 and were cultured in media containing 250 μg/mL of hygromycin B (Life Technology). To induce
448 expression of Cas9, cells were treated with 1 μg/mL of doxycycline (Clontech) for 3–5 days.
449 Clonal selection was performed by single cell dilution on 96-well plates. The individual colonies
450 were collected and the expression of Sptlc2 was examined by western-blotting using Sptlc2
451 antibody.

452 U937 SGSM1$^{-/-}$ cells were kindly provided by Sebastian Virreira Winter (Max Planck
453 Institute of Biochemistry, Munich, Germany) and the CRISPR/Cas9-mediated knock out cell lines
454 were established as described in Winter et al., 2016[42].

455

456 **Culturing of Mtb**

457 Culturing and infection of Mtb was conducted in a Biosafety-level 3 laboratory following
458 general safety guidelines. Mtb strain H37R, expressing constitutively mCherry were obtained from
459 the Fortune lab (Ragon Institute, Cambridge, MA). It was cultured at 37°C in 7H9 Broth medium
460 supplemented with 50µg/ml hygromycin B. The density of the bacteria at the time of infection is
461 between OD600 of 0.6 - 0.8.

462

463 **Mtb uptake assay**

464 For infection of THP-1 and U937 cells, the cells were seeded into a SensoPlate™ 96-Well
465 Glass-Bottom Plates (Greiner Bio-One) at a density of $1.5x10^4$ cells per well in RPMI
466 supplemented with 10% FBS, 1% PenStrep and 50ng/ml PMA at 37°C. One day after
467 differentiation, cells were treated for 3 days with 5µM myriocin or 15µM FB1. These cells were
468 then infected with a multiplicity of infection (MOI) of 10 in RPMI supplemented with 10% FBS
469 for 2 hours at 37°C.

470 For infection of RAW 264.7 and DC2.4 cells, $2.0x10^4$ cells per well were seeded into a
471 SensoPlate™ 96-Well Glass-Bottom Plates (Greiner Bio-One). 24 hour later, the cells were were
472 infected with an MOI of 10 in RPMI supplemented with 10% FBS for 2 hours at 37°C. Cells were
473 washed with PBS, and then fixed with 4% PFA over night at 4°C.

474

475 **Phagocytosis measurement assay**

476 Phagocytosis assay was performed as previously described[50]. Briefly, fixed cells were
477 washed twice with PBS and incubated in PBS for 15 min in Permeabilization Buffer (0.1% Triton

478 X-100 and 1%BSA). Cells were stained with Phalloidin-Alexa 488 (Thermo Fisher) at a final
479 concentration of 33nM for 60 min and washed one time with PBS. After the Phalloidin-staining,
480 cells were stained with DAPI for 10 mins and washed 3 times with PBS. Cells were then imaged
481 using the Keyence BZ-X700 with a PlanFluor 20x objective. The parameters for imaging were
482 kept the same for each sample. For image analysis the Keyence BZ-X Analyzer software was used.
483 In brief: The outline of the cells was determined via the Alexa488 signal (Phalloidin staining) and
484 the number and area of mCherry (Mtb) signal in the Alexa488 signal was detected by the program.
485 In a second round the number of cells was determined by counting the nuclei via the DAPI staining.
486 Number of bacteria (mCherry-signal) inside the cell was divided by the number of cells (DAPI
487 signal) to identify the phagocytosis efficiency.
488
489 **Live imaging of phagocytosis**
490 For transient transfection, RAW 264.7 cells were seeded into a SensoPlate™ 96-Well
491 glass-bottom plates at a cell number of $1.0x10^4$ cells/well 24 hours prior transfection. Transfection
492 was conducted with Lipofectamine 3000 according to manufacturer's instructions. For imaging,
493 the growth medium was aspirated and replaced with RPMI without phenol red containing Zymosan
494 A Bioparticles Alexa595 at an MOI of 10. The 96-well plates were centrifuged at 1000rpm for one
495 minute. The cells were imaged with the SDC microscope (Nikon) and 3-4 different spots per well
496 were imaged at the same time for 60 min with capture intervals of 15 sec. The parameters for
497 imaging were kept the same for each sample.
498
499 **Live image analysis (quantification)**

500 Of live cell images, individual images were selected for further analysis if they captured a
501 cell bound to a Zymosan particle while maintaining a healthy morphology throughout the imaging
502 time-course. Imaging analysis was performed using FIJI software[51]. The parameters for image
503 processing were kept constant when comparing different data sets. The area of the phagosome was
504 selected, cropped and opened in a new window. The threshold at different time points was
505 measured by the analyze-measure function of FIJI. The values for the GFP-threshold of the
506 phagosome area were divided by the values for the GFP-threshold of the whole cell at the
507 corresponding time points.
508
509 **Dectin-1 and CD45 displacement assay**
510 RAW 264.7 WT and Sptlc2$^{-/-}$ cells were seeded on glass coverslips in 12-well plates and
511 grown to 70-90% confluency overnight. Cells were transfected with pMXsIP Dectin-1-GFP
512 using Lipofectamine 3000 (Invitrogen) according to the manufacturer's instructions. After 24
513 hrs, cells were washed three times with ice-cold PBS, kept on ice for 5 min, and inoculated with
514 Alexa Fluor 594-conjugated Zymosan in chilled serum-free DMEM at a ratio of 10 beads per
515 cell. After centrifugation for 5 min at 250 x g and 4°C, cells were incubated for 5 min at 37°C,
516 washed three times with ice-cold PBS to remove unbound Zymosan, then fixed for 15 min with
517 4% paraformaldehyde.
518 Images were collected using an LSM880 confocal microscope using a PLAN APO 63x oil-
519 immersion objective and AIRY SCAN. Image analysis was performed using FIJI. Briefly, a
520 region-of-interest was defined around the Zymosan particle, and Pearson's correlation coefficient
521 between Dectin-1-GFP signal and anti-CD45-APC signal was calculated using the colocalization
522 function.

523

524 **Flow cytometry**

525 RAW 264.7 wildtype and Sptlc2$^{-/-}$ cells were rinsed with PBS and lifted from the flask
526 using treatment with trypsin. Fc receptor was blocked with CD16/32 antibody (1:100) and cells
527 were stained with ZombieAqua Live/Dead (1:200). Cells were then stained with either CD45-
528 APC (1:200), or Dectin-1-FITC (1:50) for 30 min. Finally, cells were fixed for 20 mins in 4%
529 paraformaldehyde and analyzed using an LSR-II flow cytometer. Cells independently stained
530 with ZombieAqua, CD45-APC, and Dectin-1-FITC were used for compensation. Analysis was
531 performed using FlowJo software.

532

533 **Herpes Simplex Virus-1 infection**

534 HSV-1-mCherry reporter virus was kindly provided by the lab of Dr. David Johnson
535 (Oregon Health and Science University, Portland, Oregon). Twenty-four hours prior to infection,
536 $1x10^4$ wildtype and Sptlc2 knockout RAW 264.7 cells were seeded on glass coverslips in a 12-
537 well plate. Cells were equally infected at an MOI ~1, and incubated for 12 hours at 37°C and 5%
538 CO_2. Coverslips were fixed for 20 mins in 4% paraformaldehyde, stained with DAPI and then
539 imaged on a Keyence BZ-X700. Infection rates were calculated by dividing the mCherry
540 expressing cells with the total number of cells (DAPI signal).

541

542

543

544 **References**

545

546 1. Daniel, T. M. The history of tuberculosis. *Respir. Med.* **100**, 1862–1870 (2006).

547 2. *Global tuberculosis report 2018.* (2018).

548 3. Korb, V., Chuturgoon, A. & Moodley, D. Mycobacterium tuberculosis: Manipulator of

549 Protective Immunity. *Int. J. Mol. Sci.* **17**, 131 (2016).

550 4. Ouimet, M. *et al.* Mycobacterium tuberculosis induces the miR-33 locus to reprogram

551 autophagy and host lipid metabolism. *Nat. Immunol.* **17**, 677–686 (2016).

552 5. Fine-Coulson, K., Reaves, B. J., Karls, R. K. & Quinn, F. D. The Role of Lipid Raft

553 Aggregation in the Infection of Type II Pneumocytes by Mycobacterium tuberculosis.

554 *PLoS One* **7**, (2012).

555 6. Thompson, C. R. *et al.* Sphingosine Kinase 1 (SK1) Is Recruited to Nascent Phagosomes

556 in Human Macrophages: Inhibition of SK1 Translocation by Mycobacterium tuberculosis.

557 *J. Immunol.* **174**, 3551–3561 (2005).

558 7. Levin, R., Grinstein, S. & Schlam, D. Phosphoinositides in phagocytosis and

559 macropinocytosis. *Biochim. Biophys. Acta - Mol. Cell Biol. Lipids* **1851**, 805–823 (2015).

560 8. Tafesse, F. G. *et al.* Disruption of Sphingolipid Biosynthesis Blocks Phagocytosis of

561 Candida albicans. *PLoS Pathog.* **11**, 1–27 (2015).

562 9. Malik, Z. A. *et al.* Cutting Edge: Mycobacterium tuberculosis Blocks Ca2+ Signaling and

563 Phagosome Maturation in Human Macrophages Via Specific Inhibition of Sphingosine

564 Kinase. *J. Immunol.* **170**, 2811–2815 (2003).

565 10. Gatfield, J. & Pieters, J. Essential role for cholesterol in entry of mycobacteria into

566 macrophages. *Science* **288**, 1647–50 (2000).

567 11. Kinoshita, M., Suzuki, K. G. N., Murata, M. & Matsumori, N. Evidence of lipid rafts
568 based on the partition and dynamic behavior of sphingomyelins. *Chem. Phys. Lipids* **215**,
569 84–95 (2018).
570 12. García-Arribas, A. B., Alonso, A. & Goñi, F. M. Cholesterol interactions with ceramide
571 and sphingomyelin. *Chem. Phys. Lipids* **199**, 26–34 (2016).
572 13. El Alwani, M., Wu, B. X., Obeid, L. M. & Hannun, Y. A. Bioactive sphingolipids in the
573 modulation of the inflammatory response. *Pharmacol. Ther.* **112**, 171–183 (2006).
574 14. Hla, T. & Dannenberg, A. J. Sphingolipid Signaling in Metabolic Disorders. *Cell Metab.*
575 **16**, 420–434 (2012).
576 15. Taha, T. A., Mullen, T. D. & Obeid, L. M. A house divided: Ceramide, sphingosine, and
577 sphingosine-1-phosphate in programmed cell death. *Biochim. Biophys. Acta - Biomembr.*
578 **1758**, 2027–2036 (2006).
579 16. Hakomori, S. I. & Igarashi, Y. Functional role of glycosphingolipids in cell recognition
580 and signaling. *J. Biochem.* **118**, 1091–1103 (1995).
581 17. Hannun, Y. A. & Obeid, L. M. The ceramide-centric universe of lipid-mediated cell
582 regulation: Stress encounters of the lipid kind. *J. Biol. Chem.* **277**, 25847–25850 (2002).
583 18. Snider, A. J., Alexa Orr Gandy, K. & Obeid, L. M. Sphingosine kinase: Role in regulation
584 of bioactive sphingolipid mediators in inflammation. *Biochimie* **92**, 707–715 (2010).
585 19. Leier, H. C., Messer, W. B. & Tafesse, F. G. Lipids and pathogenic flaviviruses : An
586 intimate union. 1–7 (2018). doi:https://doi.org/10.1371/journal.ppat.1006952
587 20. Capasso, S. *et al.* Sphingolipid metabolic flow controls phosphoinositide turnover at the
588 trans -Golgi network. *EMBO J.* **36**, 1736–1754 (2017).
589 21. Hinkovska-Galcheva, V., Boxer, L., Mansfield, P. J., Schreiber, A. D. & Shayman, J. A.

590 Enhanced phagocytosis through inhibition of de novo ceramide synthesis. *J. Biol. Chem.*
591 **278**, 974–982 (2003).
592 22. Hinkovska-Galcheva, V., Boxer, L., Mansfield, P. J., Schreiber, A. D. & Shayman, J. A.
593 Enhanced Phagocytosis through Inhibition of de Novo Ceramide Synthesis. *J. Biol. Chem.*
594 **278**, 974–982 (2003).
595 23. Hanada, K. Serine palmitoyltransferase, a key enzyme of sphingolipid metabolism.
596 *Biochim. Biophys. Acta* **1632**, 16–30 (2003).
597 24. Gault, C., Obeid, L. & Hannun, Y. An overview of sphingolipid metabolism: from
598 synthesis to breakdown Introduction to Sphingolipid Metabolism. *Adv Exp Med Biol* **688**,
599 1–23 (2010).
600 25. Meivar-Levy, I., Sabanay, H., Bershadsky, A. D. & Futerman, A. H. The Role of
601 Sphingolipids in the Maintenance of Fibroblast Morphology. *J. Biol. Chem.* **272**, 1558–
602 1564 (2002).
603 26. Underhill, D. M. Macrophage recognition of zymosan particles. *J. Endotoxin Res.* **9**, 176–
604 180 (2003).
605 27. Mansour, M. K. *et al.* Dectin-1 Activation Controls Maturation of β-1,3-Glucan-
606 containing Phagosomes. *J. Biol. Chem.* **288**, 16043–16054 (2013).
607 28. Rothfuchs, A. G. *et al.* Dectin-1 Interaction with Mycobacterium tuberculosis Leads to
608 Enhanced IL-12p40 Production by Splenic Dendritic Cells. *J. Immunol.* **179**, 3463–3471
609 (2007).
610 29. Wagener, M., Hoving, J. C., Ndlovu, H. & Marakalala, M. J. Dectin-1-Syk-CARD9
611 Signaling Pathway in TB Immunity. *Front. Immunol.* **9**, (2018).
612 30. Wisner, T. W., Sugimoto, K., Howard, P. W., Kawaguchi, Y. & Johnson, D. C.

613 Anterograde Transport of Herpes Simplex Virus Capsids in Neurons by both Separate and
614 Married Mechanisms. *J. Virol.* **85**, 5919–5928 (2011).
615 31. Tiwari, V. & Shukla, D. Nonprofessional Phagocytosis Can Facilitate Herpesvirus Entry
616 into Ocular Cells. *Clin. Dev. Immunol.* **2012**, 1–8 (2012).
617 32. Clement, C. *et al.* A novel role for phagocytosis-like uptake in herpes simplex virus entry.
618 *J. Cell Biol.* **174**, 1009–1021 (2006).
619 33. Gianni, T., Gatta, V. & Campadelli-Fiume, G. V 3-integrin routes herpes simplex virus to
620 an entry pathway dependent on cholesterol-rich lipid rafts and dynamin2. *Proc. Natl.*
621 *Acad. Sci.* **107**, 22260–22265 (2010).
622 34. Goodridge, H. S. *et al.* Activation of the innate immune receptor Dectin-1 upon formation
623 of a 'phagocytic synapse'. *Nature* **472**, 471–475 (2011).
624 35. Grassmé, H. *et al.* Host defense against Pseudomonas aeruginosa requires ceramide-rich
625 membrane rafts. *Nat. Med.* **9**, 322 (2003).
626 36. Mao, Y. & Finnemann, S. C. Regulation of phagocytosis by Rho GTPases. *Small*
627 *GTPases* **6**, 89–99 (2015).
628 37. Hoppe, A. D. & Swanson, J. A. Cdc42, Rac1, and Rac2 Display Distinct Patterns of
629 Activation during Phagocytosis. *Mol. Biol. Cell* **15**, 3509–3519 (2004).
630 38. Schlam, D. *et al.* Phosphoinositide 3-kinase enables phagocytosis of large particles by
631 terminating actin assembly through Rac/Cdc42 GTPase-activating proteins. *Nat. Commun.*
632 **6**, 8623 (2015).
633 39. Hanada, K. *et al.* Molecular machinery for non-vesicular trafficking of ceramide. *Nature*
634 **426**, 803–809 (2003).
635 40. Marshall, J. G. *et al.* Restricted Accumulation of Phosphatidylinositol 3-Kinase Products

636 in a Plasmalemmal Subdomain during Fcγ Receptor-Mediated Phagocytosis. *J. Cell Biol.*
637 **153**, 1369–1380 (2001).
638 41. Subbaiah, P. V. & Sargis, R. M. Sphingomyelin: A natural modulator of membrane
639 homeostasis and inflammation. *Med. Hypotheses* **57**, 135–138 (2001).
640 42. Virreira Winter, S., Zychlinsky, A. & Bardoel, B. W. Genome-wide CRISPR screen
641 reveals novel host factors required for Staphylococcus aureus α-hemolysin-mediated
642 toxicity. *Sci. Rep.* **6**, 24242 (2016).
643 43. Wegner, M. S., Gruber, L., Mattjus, P., Geisslinger, G. & Grösch, S. The UDP-glucose
644 ceramide glycosyltransferase (UGCG) and the link to multidrug resistance protein 1
645 (MDR1). *BMC Cancer* **18**, 1–10 (2018).
646 44. Viswanathan, G., Jafurulla, M., Kumar, G. A., Raghunand, T. R. & Chattopadhyay, A.
647 Macrophage sphingolipids are essential for the entry of mycobacteria. *Chem. Phys. Lipids*
648 **213**, 25–31 (2018).
649 45. Goodridge, H. S. *et al.* Activation of the innate immune receptor Dectin-1 upon formation
650 of a ˜- Phagocytic synapse-™. *Nature* **472**, 471–475 (2011).
651 46. Feng, S. *et al.* A Rapidly Reversible Chemical Dimerizer System to Study Lipid Signaling
652 in Living Cells. *Angew. Chemie Int. Ed.* **53**, 6720–6723 (2014).
653 47. BLIGH, E. G. & DYER, W. J. A rapid method of total lipid extraction and purification.
654 *Can. J. Biochem. Physiol.* **37**, 911–7 (1959).
655 48. Tafesse, F. G. *et al.* GPR107, a G-protein-coupled Receptor Essential for Intoxication by
656 Pseudomonas aeruginosa Exotoxin A, Localizes to the Golgi and Is Cleaved by Furin. *J.*
657 *Biol. Chem.* **289**, 24005–24018 (2014).
658 49. Mali, P. *et al.* RNA-guided human genome engineering via Cas9. *Science* **339**, 823–6
659 (2013).

660 50. Rashidfarrokhi, A., Richina, V. & Tafesse, F. G. Visualizing the Early Stages of
661 Phagocytosis. *J. Vis. Exp.* (2017). doi:10.3791/54646
662 51. Schindelin, J. *et al.* Fiji: an open-source platform for biological-image analysis. *Nat.*
663 *Methods* **9**, 676–682 (2012).
664
665

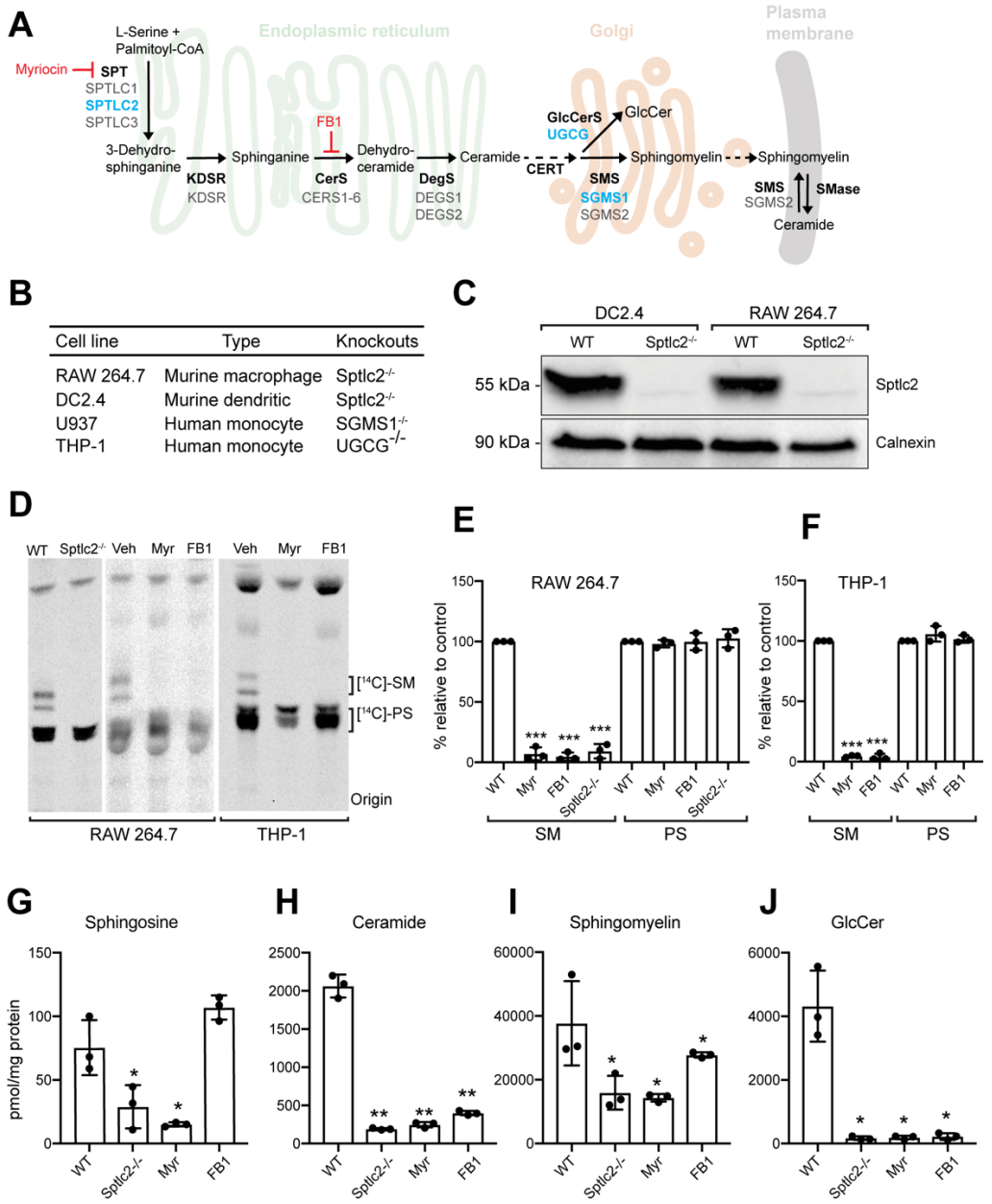

Figure 1: Manipulation of cellular sphingolipid levels using genetics and chemical tools. (A) Simplified overview of sphingolipid biosynthetic pathway. Genes that are deleted using CRISPR/Cas9 system are indicated in blue and the inhibitors that are used in this study are shown in red. (B) Model phagocyte cell lines used in this study, respective species background, and genetic knockouts available. (C) Western blot probed using anti-Sptlc2 antibody in wildtype and CRISPR/Cas9 knockout DC2.4 and RAW 264.7 cells (upper), and probed against calnexin as loading control (lower). (D) Control, mutant and inhibitor-treated cells were labeled with the sphingolipid precursor 3-L-[^{14}C]-serine, and total lipids were extracted and analyzed by thin layer chromatography (TLC) and autoradiography. (E, F) Quantification of the [^{14}C]-SM and [^{14}C]-PS signals from [^{14}C]-serine labeling of RAW264.7 and THP-1 cells shown in *D*. (G-J) Total lipids were extracted from control, Sptlc2$^{-/-}$ and inhibitor-treated cells and lipid profiling was performed using LC/MS. Levels of sphingosine (G), ceramide (H), sphingomyelin (I) and glucosylceramide (GlucCer) are shown. All graphs display SD of three independent experiments, and an unpaired t-test was used to analyze the significance of the data. *$p<0.05$, **$p<0.01$, *** $p < 0.001$.

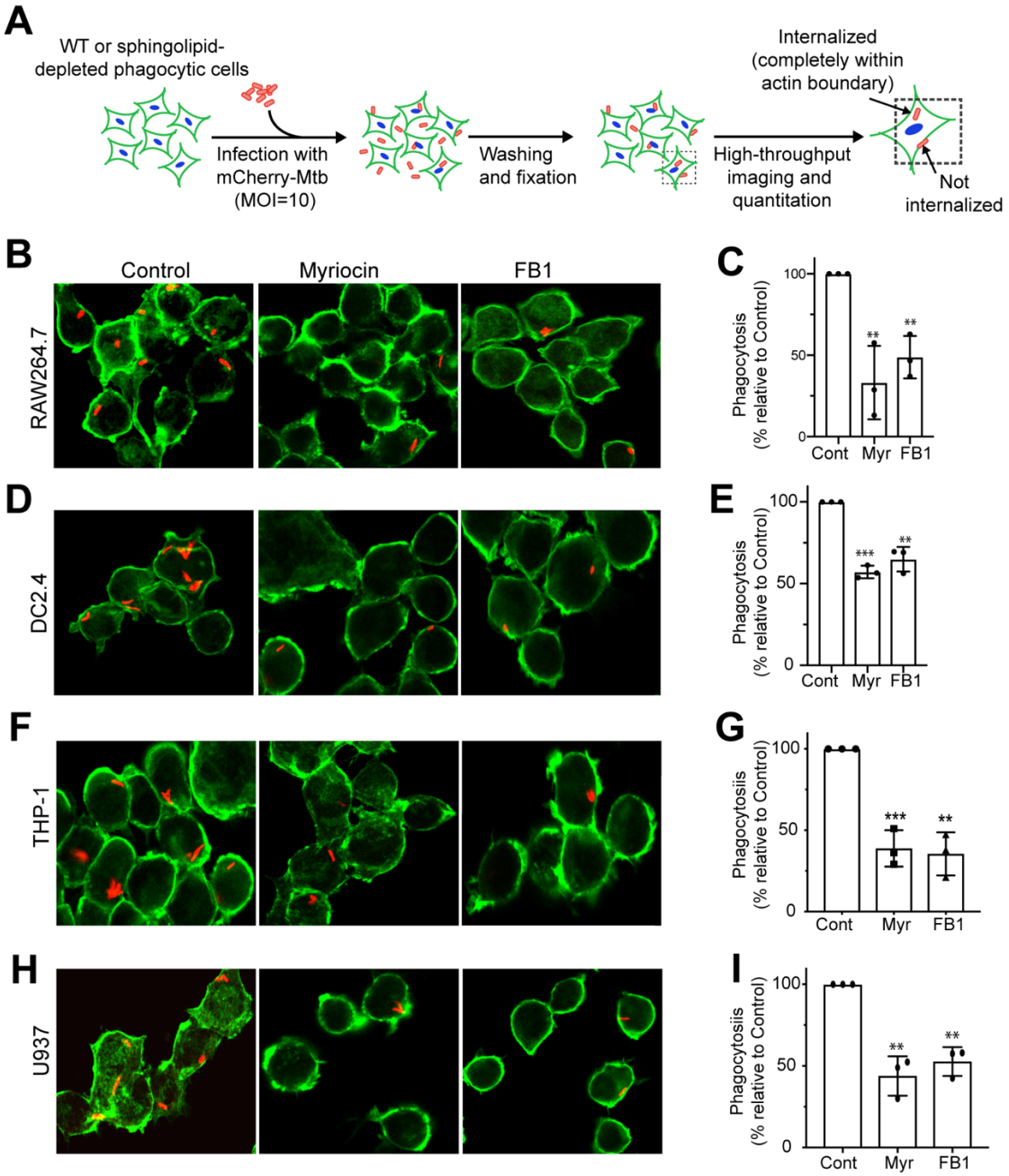

Figure 2: Sphingolipid biosynthesis is required for efficient phagocytosis of Mtb. (A) Overview of the phagocytosis experiment. (B, D) Representative images of Mtb-infected RAW 264.7 (B) and DC2.4 (D) cells. (C, E) Quantification of Mtb uptake in RAW 264.7 (C) and DC2.4 (E) cells. (E, H) Representative images of infected THP-1 (F) and U937 (H) monocyte-derived macrophages. $2x10^4$ THP-1 and U937 cells were plated in 96-well plate and were differentiated using 80ng/ml PMA for one day, and then treated for three days with myriocin or FB1. (G, I) Quantification of Mtb uptake in THP-1 (G) and U937 (I) cells. Three independent experiments were performed each in triplicate with at least 1,000 cells quantified per replicate. Mtb uptake was defined using total number of bacteria (mCherry signal) within cellular periphery (Phalloidin-Alexa488 signal) and cellular counts were defined by nuclear stain. Data are mean ± SD. ***p<0.001, two-tailed unpaired t-test. Data are mean ± SD. **p<0.01, ***p<0.001, two-tailed unpaired t-test.

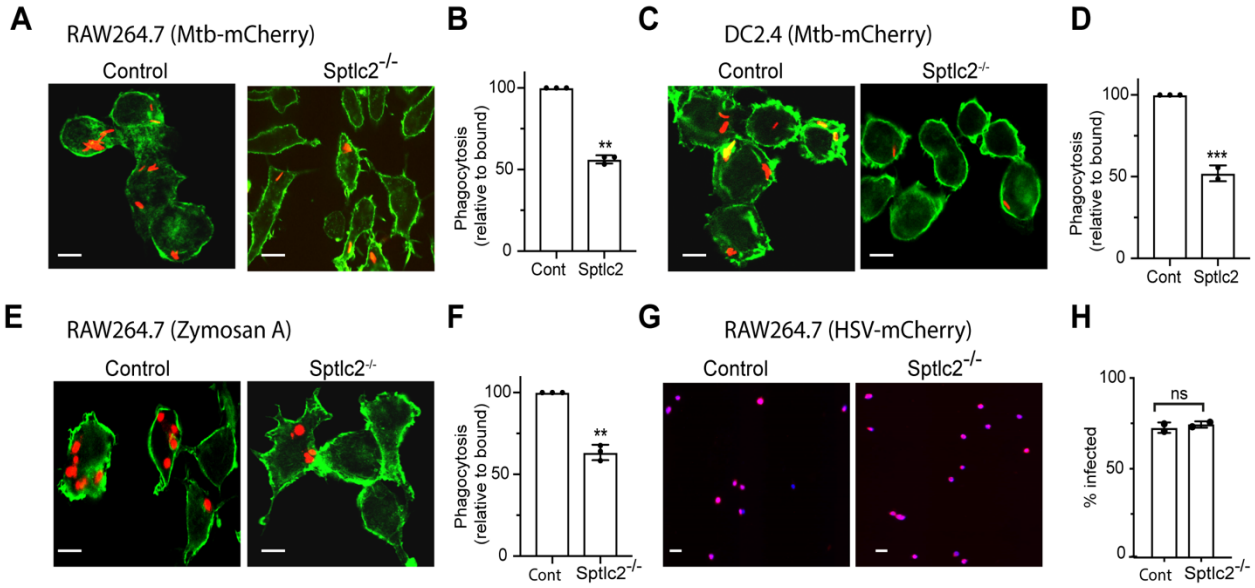

692

693 **Figure 3: Sphingolipid biosynthesis is required for efficient phagocytosis of Mtb and Zymosan A, but**
694 **not for HSV entry.** (A) Representative images of wildtype and Sptlc2$^{-/-}$ RAW 264.7 (A) and DC2.4 (C)
695 cells infected with mCherry-expressing Mtb. (B, D) Quantification of Mtb uptake for experiments
696 performed as in *A* and *C*, respectively. (E) Representative images of wildtype and Sptlc2$^{-/-}$ RAW 264.7 cells
697 infected with Alexa fluor 594-conjugated Zymosan A particles. (F) Quantification of Zymosan A uptake
698 uptake performed as in *E*. (G) Microscopy images of cells that were infected with HSV-mCherry (MOI of
699 10). At 12 h post infection, cells were fixed, stained with DAPI and analyzed by microscopy. (H)
700 Quantification of experiments performed as described *G*. Three independent experiments were performed
701 each in triplicate with at least 1,000 cells quantified per replicate. Data are mean ± SD. ***p<0.001, two-
702 tailed unpaired t-test. Data are mean ± SD. **p<0.01, ***p<0.001, ns = not significant, two-tailed unpaired
703 t-test.
704

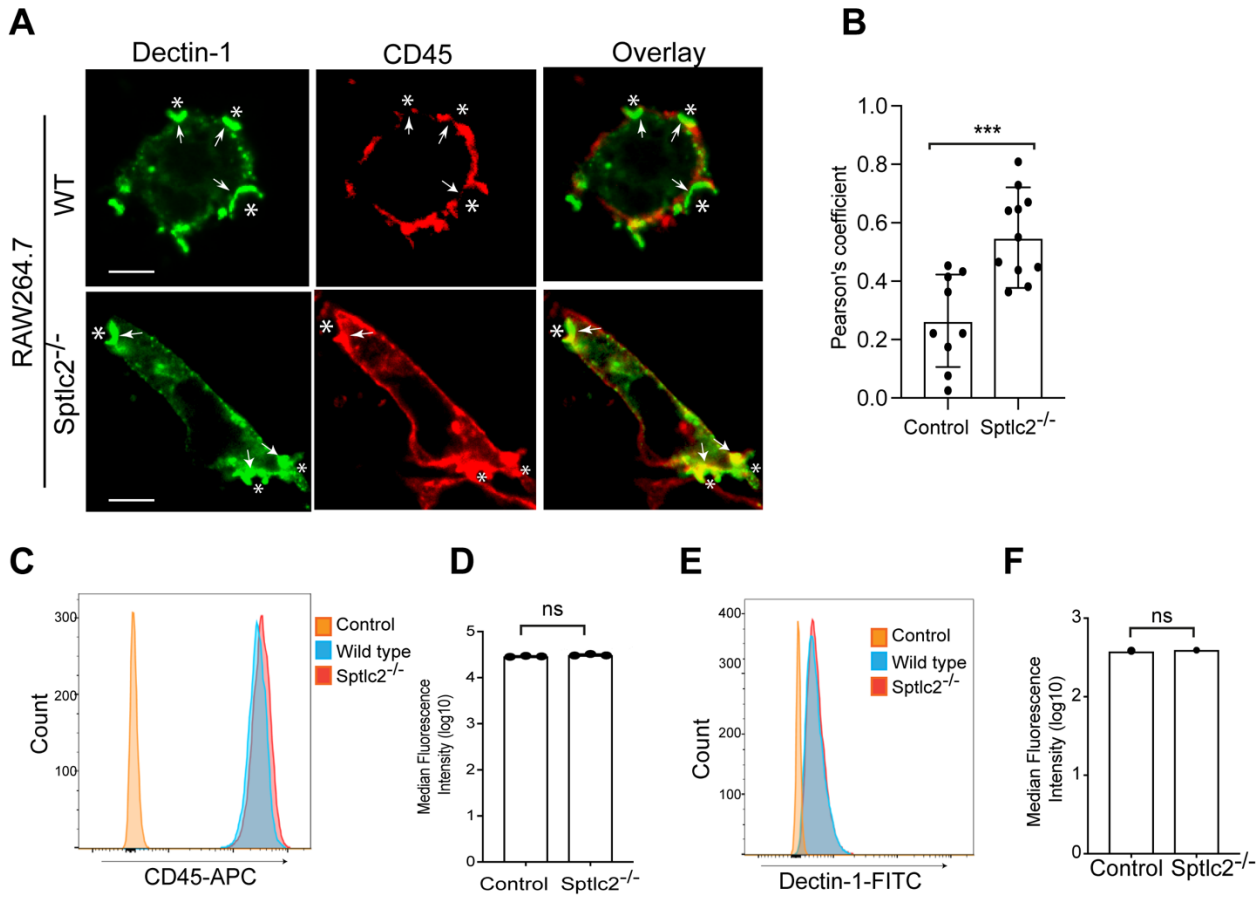

Figure 4: Exclusion of CD45 by Dectin-1 from the cup formation site is impaired in Sptlc2$^{-/-}$ cells. (A) Confocal microscopy of GFP-tagged Dectin-1-expressing RAW264.7 macrophages stimulated with Zymosan A for 2 min and stained for CD45 (red). Zymosan particles are shown in star (*) at the phagocytic cup. (B) Colocalization measurement of CD45 and Dectin-1 at the site of cup formation as presented by Pearson's colocalization coefficient. (C, E) Flow cytometry of wildtype and Sptlc2$^{-/-}$ RAW264.7 cells that were stained for CD45 and Dectin-1at the cell surface. (D, F) Graphs showing quantification of cell surface expression of the receptors described in *C* and *E*, respectively. All data are representative of 3 independent experiments performed in triplicate. Data are mean ± SD. ns = not significant, two-tailed unpaired t-test.

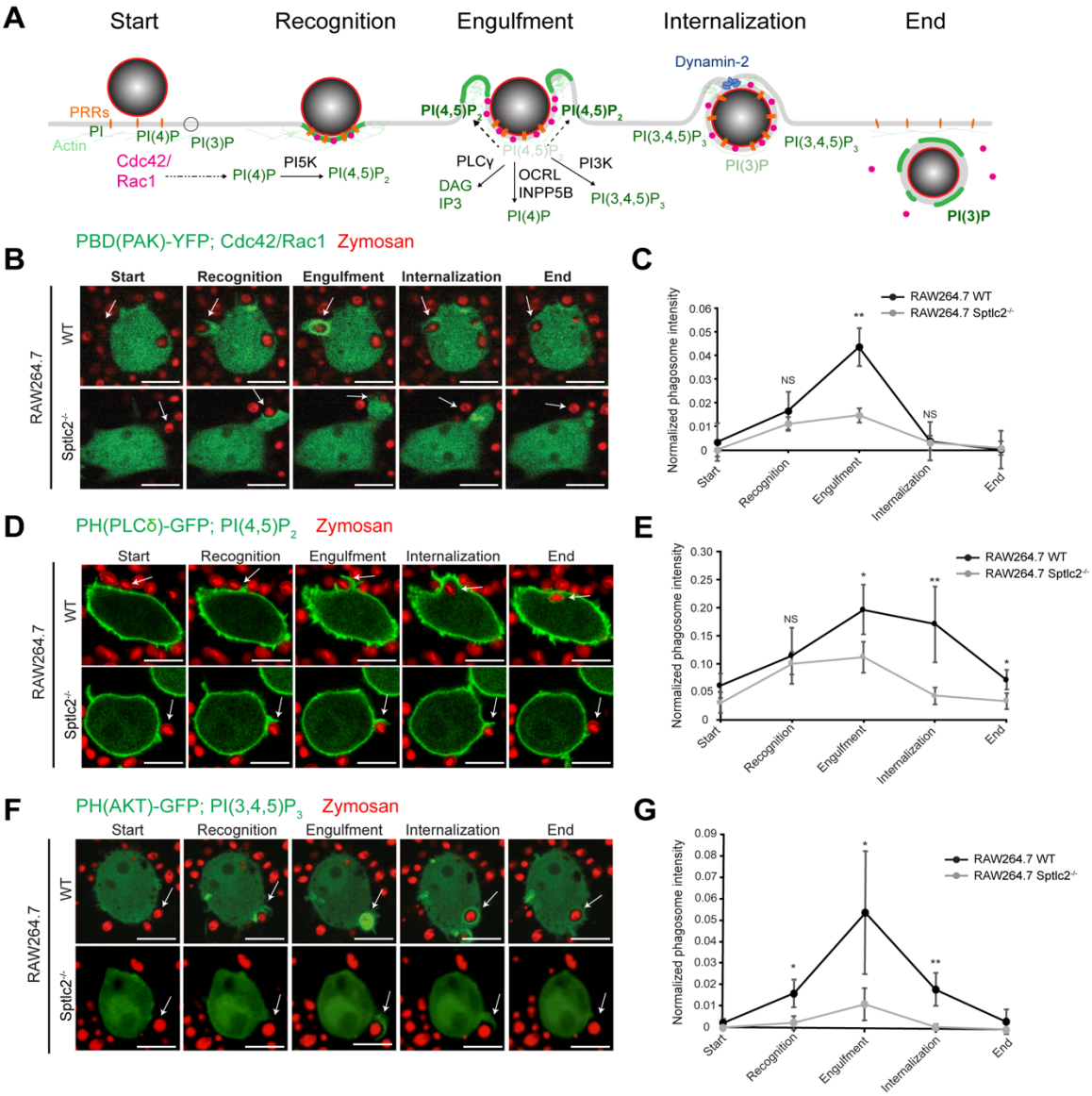

Figure 5. Sphingolipids are essential for efficient recruitment of Rac1/Cdc42 and phosphoinositide turnover at the phagocytic cup. (A) Schematic representation of the small GTPase Rac1/Cdc42 and phosphoinositide dynamics during phagocytosis. (B) Confocal images of wild type and Sptlc2$^{-/-}$ RAW264.7 cells transfected with PAK(PBD)–GFP, a biosensor for active Rac1/Cdc42, during phagocytosis. Cells were incubated with Alexa fluor 594-conjugated Zymosan A particles, and live imaging was performed. Images captured at 30-second intervals are shown. (C) A graph showing quantitation of the PAK(PBD) fluorescence intensity in the course of formation of a phagocytic cup (shown in arrow) as performed in *B*. (D, F) Time-lapse confocal microscopy images of wildtype and Sptlc2$^{-/-}$ RAW 264.7 cells expressing PH(PLCδ)-GFP, the PI(4,5)P_2 biosensor (D) or PH(AKT)-GFP, the (PI3,4,5)P_3 biosensor (F) after infection with Alexa flour 594 conjugated Zymosan A particles at MOI of 10. Representative images that are captured at 30-second intervals are shown. (E, G) Accumulation of GFP signal to site of particle binding was quantified by the ratio of GPF signal intensity at phagosome versus GFP signal across entire cell at the indicted time points for experiments performed as *D* and *F*. n= 3 independent experiments and the mean GFP intensity profiles of 10 - 20 cells are represented. Data are mean ± SD. *p<0.05, **p<0.01, two-tailed unpaired t-test, ns = not significant

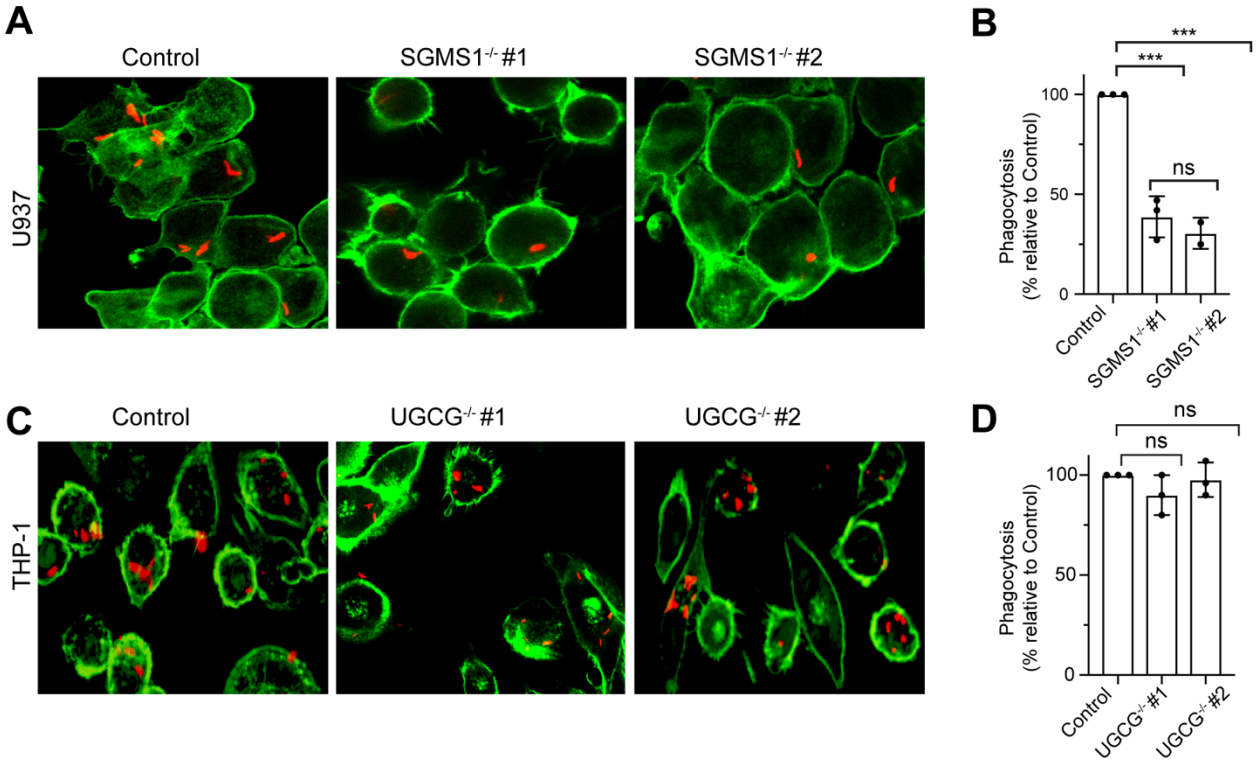

732

733 **Figure 6: SGMS1$^{-/-}$ cells, but not UGCG$^{-/-}$, are defective in phagocytic uptake of Mtb.**
734 (A, C) Representative images of wildtype and two clonal isolates of SGMS1 CRISPR/Cas9 knockout
735 U937 cells (A) and THP-1 cells deficient in UGCG (Glucosylceramide synthase) gene infected with
736 mCherry-expressing Mtb. Cells were activated with 80nM PMA for 24 h before Mtb infection. (B, D)
737 Quantification of Mtb uptake for experiments described as in *A* and *C*, respectively. Three independent
738 experiments were performed each in triplicate with at least 1,000 cells quantified per replicate. Data are
739 mean ± SD. ***$p<0.001$, ns = not significant, two-tailed unpaired t-test.
740
741

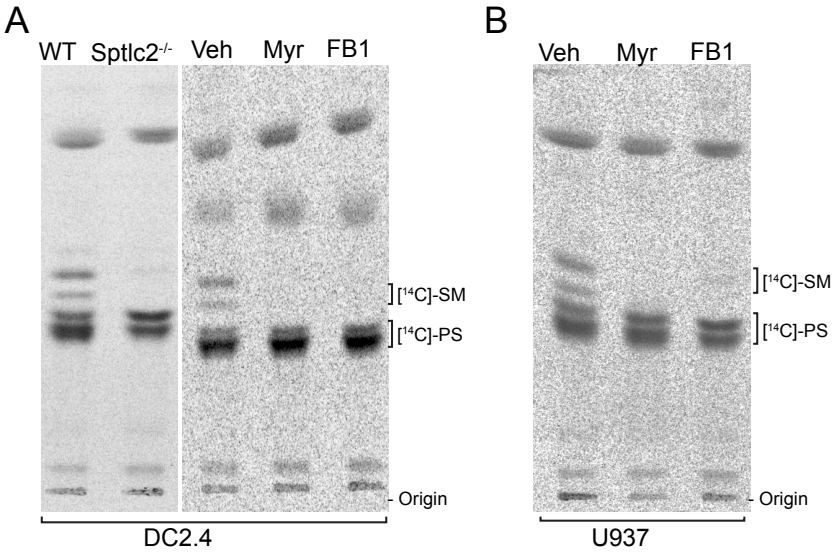

Supplemental Figure 1: Genetic and small molecule inhibitors mediated depletion of sphingolipid in phagocytes. (A, B) Control, mutant and inhibitor-treated cells were labeled with the sphingolipid precursor 3-L-[^{14}C]-serine, and total lipids were extracted and analyzed by thin layer chromatography and autoradiography. All data are representative of 3 independent experiments.

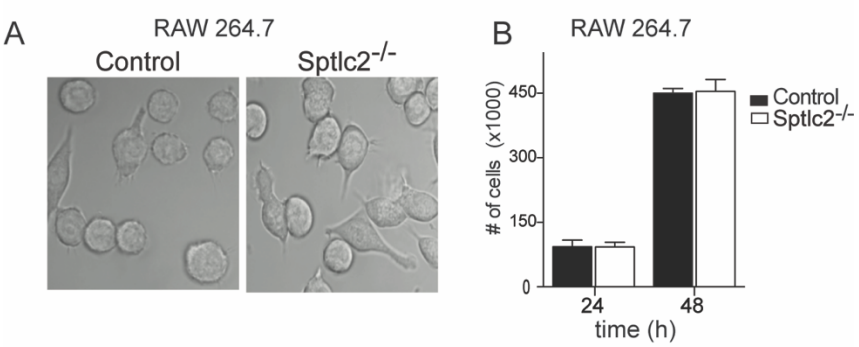

Supplemental Figure 2: Depletion of sphingolipids has no effect on cell morphology, growth rate or cell division. (A) Microscopy images of control and Sptlc2$^{-/-}$ RAW 264.7 macrophages, showing no morphological difference between the mutant and control cells. (B) The cell division of the control and Sptlc2$^{-/-}$ RAW 264.7 macrophages at different time points was measured and presented.